METHODOLOGY FOR INVESTIGATING THE INTERFERENCE IMMUNITY OF SATELLITE NAVIGATION ANTENNA ARRAYS USING ANSYS HFSS

Vadym Slyusar
Central Research Institute of Armaments and Military Equipment of Armed Forces of Ukraine, Kyiv, Ukraine
swadim@ukr.net

Igor Atamanyuk [1,2]
[1] Warsaw University of Life Sciences, Warsaw, Poland
[2] Mykolaiv National Agrarian University, Mykolaiv, Ukraine
ihor_atamaniuk@sggw.edu.pl

Ihor Sliusar
Department of Information Systems and Technologies
Poltava State Agrarian University, Poltava, Ukraine
islyusar2007@ukr.net

Zakhar Shelemin
Scientific Research Department
Central Research Institute of Armaments and Military Equipment of Armed Forces of Ukraine, Kyiv, Ukraine
zarshel@gmail.com

Ievgen Sidenko
Department of Intelligent Information Systems
Petro Mohyla Black Sea National University, Mykolaiv, Ukraine
ievgen.sidenko@chmnu.edu.ua

Yuriy Kondratenko [1,2]
[1] Petro Mohyla Black Sea National University, Mykolaiv, Ukraine
[2] Institute of Artificial Intelligence Problems, Kyiv, Ukraine
yuriy.kondratenko@chmnu.edu.ua

KEYWORDS
Digital antenna array (DAA), controlled reception pattern antennas (CRPA), Ansys HFSS, modelling

ABSTRACT

This paper presents an HFSS-based procedure for quantifying the interference resilience of satellite-navigation antennas on autonomous platforms that employ digital antenna arrays and controlled reception pattern antennas (CRPAs). An individual element is first simulated to determine the operating band under the VSWR<2 criterion and to select the analysis frequency. The complete array is then solved with in-phase excitation to obtain the zenith peak gain P. Next, a phase distribution that enforces a zenith null is identified, the associated gain depression D is measured, and interference suppression is expressed as P−D. The workflow is demonstrated on navigation CRPAs of several topologies. A six-element ring yields a relative null depth of about 36.5 dB, whereas a seven-element ring provides up to 45 dB of suppression. The strongest performance is achieved by a dual-ring 16-element array, reaching a 53 dB null depth. A square 4×4 array is lower by 8.5 dB. In further research, it would be advisable to experimentally test the influence of phase errors and also to extend this approach to other electromagnetic simulators.

INTRODUCTION

One of the salient trends in the development of autonomous vehicles (Kondratenko et al. 2022; Slyusar et al. 2024; Tijani 2022; Tu et al. 2022) is the deployment of satellite-navigation equipment. Such systems (GNSS) enable adherence to a prescribed route and help to prevent collisions with stationary obstacles. To improve the interference resilience of satellite navigation on autonomous platforms, digital antenna arrays (DAAs) (Slyusar 1999) and controlled reception pattern antennas (CRPAs) are widely employed. From DAA theory it is known that an N-element array can, in principle, place nulls in its radiation pattern in up to N−1 directions towards active jamming sources. Another key indicator of interference resilience is the instantaneous linear dynamic range of the receiver front-end (Slyusar 2004). This metric is constrained, inter alia, by inter-channel non-identity (Slyusar 1999), timing jitter (Bondarenko et al. 2011), and the resolution of the analogue-to-digital converters (ADCs) used in the channels (Slyusar 2004). In practice, however, a critical and nontrivial problem is to assess the depth of the radiation-pattern null that is potentially achievable. As a solution, this paper proposes a procedure for estimating the maximum attainable null depth based on full-wave modelling of the antenna array in the Ansys HFSS electromagnetic simulator (Ansys HFSS). The aim is not only to describe the procedure itself, but also to demonstrate its application through a study of the interference resilience of real DAA/CRPA samples of different configurations.

RELATED WORKS

The vulnerability of GNSS to deliberate interference has sustained interest in antenna systems that operate as spatial filters. These systems enable adaptive radiation-pattern control, including interference suppression by placing a null in the direction of arrival. The literature emphasises that performance depends not only on the weight computation algorithm, but also on the fidelity of the array model, and related implementation factors.

Recent studies further highlight mutual coupling and aperture non-uniformities, which distort the steering vector and make "ideal" phase laws unreliable unless the specific antenna's electromagnetic model is accounted for, effectively linking algorithm design with full-wave simulation. A substantial body of work addresses GNSS interference-mitigation algorithms, including classical linearly constrained minimum-variance methods and variants that reduce dependence on accurate a priori information about directions of arrival or interference statistics.

A common approach evaluates interference suppression indirectly via navigation-solution quality, for instance by counting how many satellites in a constellation remain usable under interference (De Lorenzo et al. 2006; Konin et al. 2023). However, a more complete assessment of a given

DAA is obtained by directly estimating the null depth in the interference direction. In (Byun et al. 2016), this is analysed for a 10-element CRPA, although that design assumes identically oriented circularly arranged patch elements, whereas modern CRPAs typically rotate each element about its normal and may employ diverse patch implementations. Consequently, a clear trend is to combine signal processing with more realistic physical antenna models, replacing idealised steering vectors with measured or numerically derived element patterns and frequency-dependent characteristics.

The authors' approach aligns with this evolution by using electromagnetic analysis not only for matching and band identification, but also for deriving realistic array patterns under different excitations, enabling estimation of attainable null depth, its sensitivity to errors, and rigorous cross-comparison of arrays and phase distributions in terms of interference protection.

PROPOSED APPROACH FOR ANTENNA MODELING

The proposed methodology for investigating interference resilience comprises three modelling stages. In the first stage, after measuring all geometric dimensions of the physical antenna system and its constituent parts, a single antenna element is modelled in Ansys HFSS. The purpose of this stage is to determine the antenna's operating frequency range so that its limits can be taken into account when selecting the simulation frequency for subsequent calculations. The corresponding passband limits are identified using a previously validated approach in which the operating range is defined by the frequencies over which the VSWR does not exceed 2.0 (Sliusar et al. 2018; Sliusar et al. 2019a; Sliusar et al. 2019b). To improve the reliability of this stage, it is advisable to complement the simulations with experimental measurements of the amplitude–frequency response of the antenna elements. The second stage consists in building a model of the entire antenna array as an integrated system and forming its radiation pattern under in-phase excitation of all elements. The task at this stage is to determine the maximum array gain in the direction of the main-beam peak, aligned with the normal to the array plane. Hereafter, this direction is referred to as the zenith. The maximum gain P is obtained from the two-dimensional radiation-pattern plot. In the final stage, the excitation phases of the array elements are adjusted so as to produce a null in the zenith direction in the array radiation pattern. From the corresponding two-dimensional gain distribution, the depth of the gain depression D in the zenith direction is then determined. The interference-resilience metric is finally defined as the difference between the in-phase main-beam maximum P and the estimated null depth D. This value characterises the potential interference suppression, since the null depth will generally decrease when steering the null towards other directions. It should be noted that, for certain array topologies and a fixed physical configuration, more than one phase distribution may yield a zenith null. Consequently, all feasible solutions should be explored in modelling in order not to overlook the optimal phase setting. The following section presents specific examples of applying the proposed methodology to evaluate the interference resilience of production navigation CRPAs manufactured in China.

SIMULATION RESULTS

One of the comparatively simple array configurations considered is a seven-element design comprising a ring of six peripheral radiating elements with a single element at the centre (Figure 1). As the central element is not involved in forming the radiation-pattern depression, the assessment of potential interference resilience was conducted using only the model of the peripheral ring array (Figure 1).

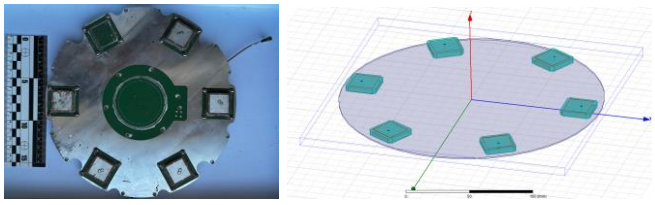

Figure 1: Seven-Element CRPA and its Model

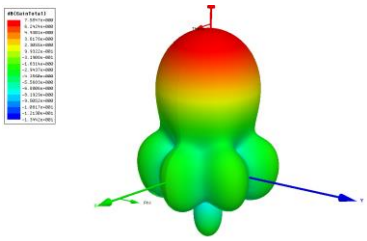

Figure 2: 3D Radiation Pattern of the Six-Element Ring DAA

Modelling of the antenna element for this CRPA established that the resonant frequency within the operational band is 1.575 GHz for a ceramic substrate with a relative permittivity of 20.9. This operating band is consistent with experimental VSWR measurements obtained for the element. With in-phase excitation of all elements, a null is formed in the zenith direction. Conversely, applying a progressive 60° phase shift when stepping sequentially around the ring from one patch antenna to the next produces a radiation-pattern maximum in the zenith direction. When the main beam is steered to zenith, the half-power beamwidth is ±23° at the −3 dB level relative to the peak value (7.5 dB). The overall null depth in the zenith direction reaches approximately −36.5 dB with respect to the maximum.

A more complex navigation DAA configuration is obtained by moving to a seven-element peripheral ring (Figure 4).

To analyse the radiation pattern of this array, a seven-port feeding network was employed. All seven ports delivered 1 W signals, with in-phase excitation applied to the seven antenna elements. This excitation corresponds to the formation of a radiation-pattern null in the zenith direction. The resulting null depth reaches −36 dB, and the −3 dB null width is approximately 30°. A zenith-directed pattern maximum can be obtained when the inter-element phase shift increases sequentially by $2\pi/7$ radians, that is, approximately 51.43°.

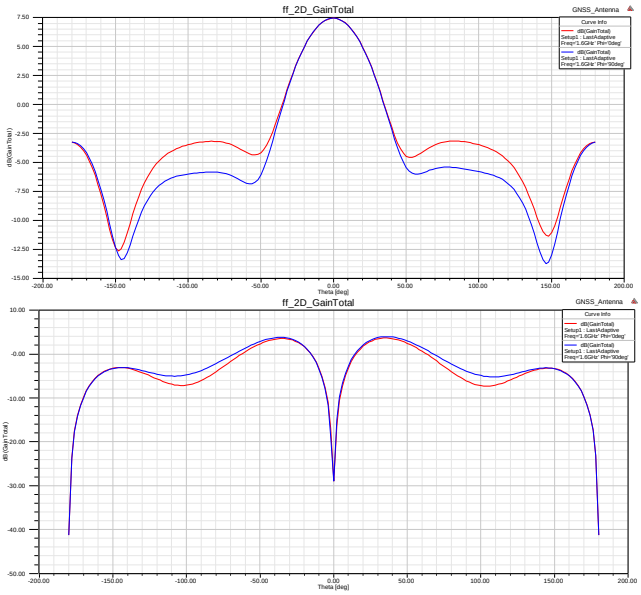

Figure 3: 2D Radiation Patterns of the Six-Element Ring Antenna Array

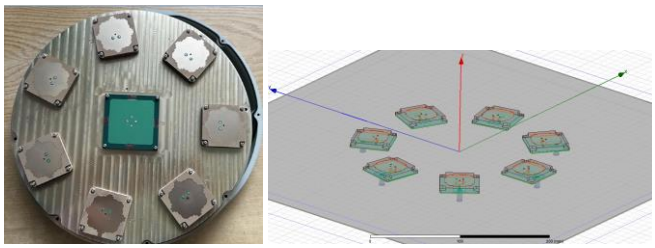

Figure 4: Eight-Element CRPA and its Model

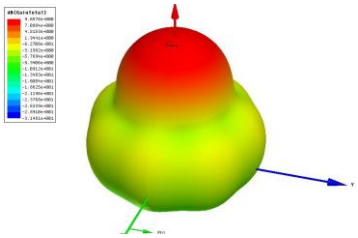

Figure 5: 3D Radiation Pattern of the 7-Element Ring DAA

Under this progressive phasing, the peak sidelobe level is −13 dB relative to the main-beam maximum (Figure 6). When referenced to the main-lobe peak gain, the overall interference suppression is approximately 45 dB. In this configuration, a phasing accuracy deviation of ±1° has a negligible effect on the spatial selectivity of the CRPA.

A substantial improvement in the interference resilience of a ring-topology GNSS DAA can be achieved by increasing the number of antenna elements to 16. One such CRPA configuration is shown in Figure 7. The topology is formed by arranging 10 elements in an outer ring and six elements in an inner ring. With appropriately coordinated phase shifts at the array-element outputs, the peak gain of the antenna in the main-beam maximum is 12.5 dB (Figure 8). The maxima of the first sidelobes are at approximately −9.5 dB relative to the main-lobe peak.

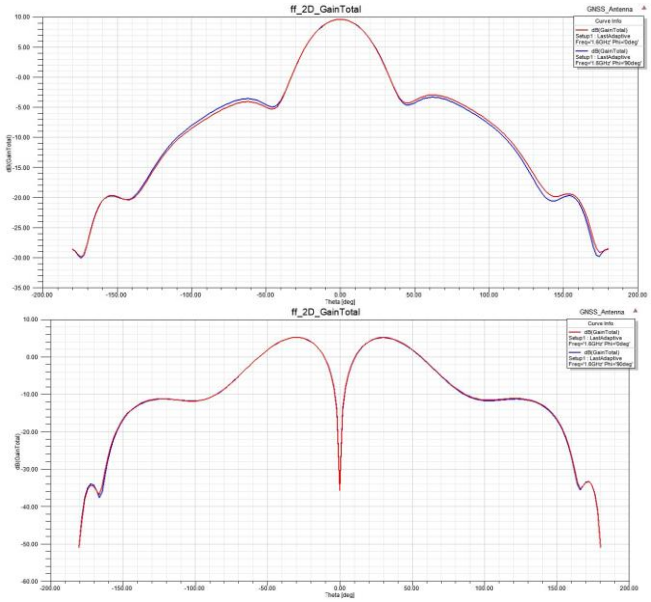

Figure 6: 2D Radiation Patterns of the 7-Element Ring DAA

The corresponding progressive phase shift across the outer ring is 36°, while for the inner ring it increases to 60°. The calculated two- and three-dimensional radiation patterns for this case are presented in Figures 8 and 9.

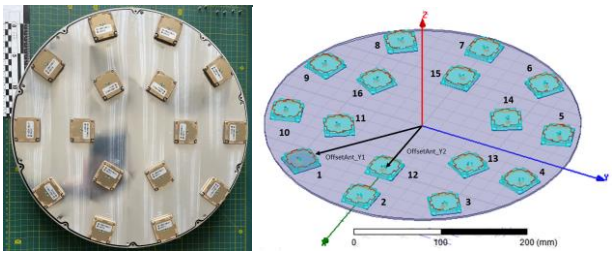

Figure 7: 16-Element CRPA and its Model

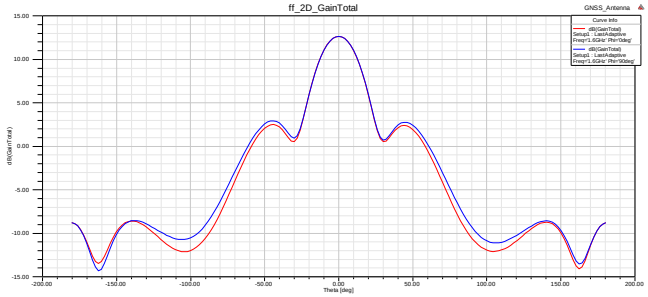

Figure 8: 2D Radiation Pattern of the 16-Element Ring DAA

Under in-phase excitation of all array elements, the signals of equal power applied to the elements of both rings have identical phases, which enables interference to be suppressed from the zenith direction. The corresponding calculated two- and three-dimensional radiation patterns are shown in Figures 9 and 10. In this case, the zenith null depth relative to the initial maximum is −53 dB (12.5 + 40.5 dB), which exceeds the relative null depth of the eight-element CRPA in Figure 4 by more than 8 dB.

In the final modelling stage, a square DAA comprising a 4×4 element arrangement was investigated. Its physical

appearance and the corresponding simulation model are shown in Figure 11.

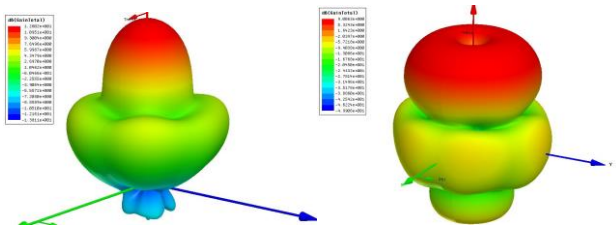

Figure 9: 3D Radiation Patterns of the 16-Element Ring Antenna Array

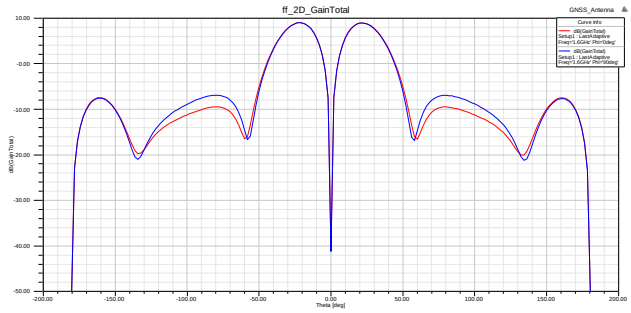

Figure 10: 2D Radiation Pattern that enables Interference to be suppressed from the Zenith Direction

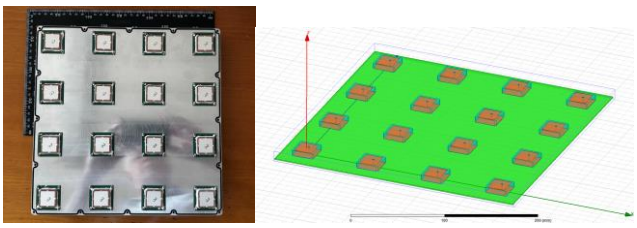

Figure 11: A Square 16-Element Antenna Array in a 4×4 Configuration and its Model

A simulation frequency of 1.6 GHz was used to form the radiation pattern. Under in-phase excitation, the main lobe was directed along the normal to the array aperture, with a peak gain of P = 14.2 dB (Figure 12).

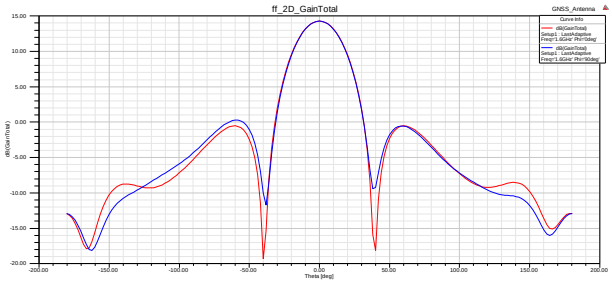

Figure 12: 2D Radiation Pattern of the 16-Element Square Antenna Array

Three phase-distribution schemes were employed to form a radiation-pattern null. In the first scheme, the DAA was notionally partitioned into four 2×2 subarrays. Within each subarray, the excitation phase was incremented by 90° when moving from one element to the next while traversing the subarray elements clockwise. The same 90° phase progression was then applied between the subarrays, treating each subarray as an equivalent single radiating element. This hierarchical phasing produced a relatively broad zenith depression, as shown in Figure 14.

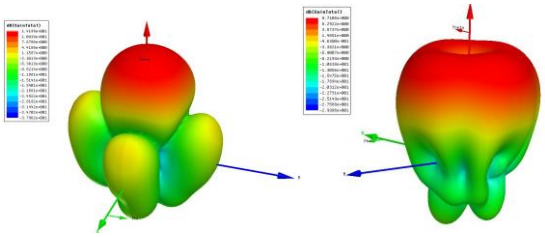

Figure 13: 3D Radiation Pattern of the 16-Elements Square Antenna Array

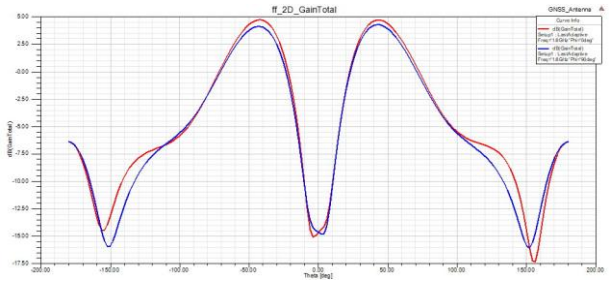

Figure 14: 2D Radiation Pattern that enables Interference to be suppressed from the Zenith Direction (1st Variant)

In the second null-forming configuration (Figure 15), the elements within all subarrays are excited in phase, for example with a zero-phase reference, while an additional 90° phase rotation is applied only at the subarray level as the subarrays are traversed clockwise.

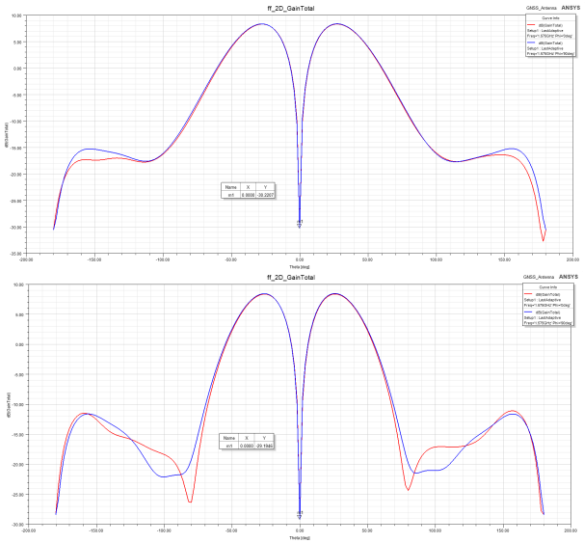

Figure 15: 2D Radiation Patterns that enables Interference to be suppressed from the Zenith Direction (2nd (Top) and 3rd Variants (Bottom))

An alternative null-forming approach mirrors that used for the dual-ring 16-element antenna (Figure 7). Specifically, a 2×2 subarray is notionally placed at the centre of the square DAA, serving as an analogue of the inner six-element ring in Figure 7. Within this central subarray, the excitation phase is

rotated by 90° when progressing from one element to the next. The remaining 12 elements of the square array, outside the central subarray, constitute an outer contour, a square frame that corresponds to the outer ten-element ring array (Figure 7). Along this outer square frame, as the elements are traversed clockwise, the phase is increased in discrete steps of 360/12 = 30° relative to the preceding element. This phasing scheme yields a zenith-pattern depression of approximately −30.22 dB (Figure 15).

CONCLUSIONS

Moving to a square antenna array in a 4×4 configuration halves the main-lobe beamwidth relative to a comparable four-element 2×2 DAA, thereby improving the ability to reject interference arriving from outside the main beam. The increased number of radiating elements, together with the symmetry of the square-array topology, enables several alternative phase-excitation schemes to be considered for forming a radiation-pattern null along the normal to the array aperture. Phase scheme 1, owing to its hierarchical phase-allocation principle, produces a relatively broad depression in the zenith direction; however, its null depth is inferior to that obtained with phase schemes 2 and 3. Phase schemes 2 and 3 yield broadly comparable null depths along the normal direction, although scheme 2, which applies in-phase excitation at the subarray level, is marginally superior, providing a null that is deeper by approximately 1 dB. By contrast, scheme 3 is characterised by a more azimuthally uniform radiation pattern when the zenith null is imposed.

It should be noted that, in terms of achievable null depth, the square 16-element array underperforms a dual-ring array with the same number of elements, a result that was not apparent a priori. Specifically, the zenith null depth relative to the original peak is −53 dB for the dual-ring CRPA (12.5 + 40.5 dB), whereas, for the square array, the best-performing null-forming option yields 44.42 dB (14.2 + 30.22 dB). This difference of more than 8.5 dB favours the dual-ring DAA as the preferable configuration. Nevertheless, these modelling outcomes require experimental validation, particularly because the square DAA exhibits a main-beam peak that is approximately 1.7 dB higher than that of the dual-ring array.

A further research direction is to analyse the influence of phase-distribution errors across the DAA aperture. Building an appropriate dataset would enable the magnitude of this influence to be predicted using neural networks (Gajbhiye et al., 2025; Kondratenko et al. 2019; Striuk et al. 2021) and would also support parametric optimisation (Kondratenko et al. 2019). To accelerate the requisite simulations, a dedicated script for automated modification of the array model (CST 2024 Python) should be employed. The proposed methodology can be extended to other electromagnetic simulators, including CST and FEKO (Altair Feko).

REFERENCES

Altair Feko, https://altair.com/feko.

Ansys HFSS, https://www.ansys.com/products/electronics/

Assessment of Ultra-Wideband (UWB) Technology, OSD/DARPA Ultra-Wideband Radar Review Panel. 1990. Battelle Tactical Technology Center, Contract No. DAAH01-88-C-0131, ARPA Order 6049.

Bankov, S. and Kuruschin, A. 2009. Raschet antenn i SVCH struktur s pomoshchyu HFSS Ansoft [Calculation of antennas and microwave structures using HFSS Ansoft.]. Moscow.

Bondarenko M., Slyusar V. 2011. Influence of jitter in ADC on precision of direction-finding by digital antenna arrays. *Radioelectronics and Communications Systems*, 54 (8), pp. 436 - 445.

Byun, G. et al. 2016. Optimum Array Configuration to Improve Null Steering Time for Mobile CRPA Systems, Journal of electromagnetic engineering and science. Korean Institute of Electromagnetic Engineering and Science. pp. 74–79.

CST 2024 Python Automation Walkthrough - AI Prompt, https://www.3ds.com/products/simulia/cst-studio-suite.

Gajbhiye, P., Singh, S., Sharma, M. 2025. A comprehensive review of AI and machine learning techniques in antenna design optimization and measurement. Discov Electron 2, 46.

Kondratenko, Yu.P., Kozlov, A.V. 2019. Parametric optimization of fuzzy control systems based on hybrid particle swarm algorithms with elite strategy. *Journal of Automation and Information Sciences.* 51(12), pp. 25-45.

Kondratenko, Y.; Atamanyuk, I.; Sidenko, I.; Kondratenko, G.; and Sichevskyi, S. 2022. Machine Learning Techniques for Increasing Efficiency of the Robot's Sensor and Control Information Processing. *Sensors*, 22(3), 1062.

Konin, V., Averyanova, Y.; Ishchenko, O. 2023. Antenna Array Application to Support Operation of GNSS Receivers under Interfering Signals. Radioelectron.Commun.Syst. 66, 305–314.

De Lorenzo, D., et al. 2006. Navigation accuracy and interference rejection for an adaptive GPS antenna array. Proc. ION GNSS, 2006, 763–773.

Sliusar, I., Slyusar, V., Voloshko, S., Zinchenko, A., Degtyareva, L. 2019a. Synthesis of quasi-fractal ring antennas, in IEEE 6th Int. Sci.-Practical Conf. "Problems of Infocommunications. Science and Technology" (PICS&T'2019), Kyiv, Ukraine, pp. 741–744.

Sliusar, I., Slyusar, V., Voloshko, S., Degtyareva, L. 2019b. Antenna synthesis based on fractal approach and DRA technologies, in IEEE 2th Ukraine Conf. on Electrical and Computer Engineering (UKRCON-2019), Lviv, Ukraine, pp. 29–34.

Sliusar, I., Slyusar, V., Voloshko, S., Smolyar, V. 2018. Synthesis of quasi-fractal hemispherical dielectric resonator antennas, 2018 IEEE 5th Int. Sci.-Practical Conf. "Problems of Infocommunications. Science and Technology" (PICSST'2018), Kharkiv, Ukraine, pp. 313–316.

Slyusar, V. I. 1999. Accuracy measurement of angular coordinates by a linear digital antenna array for nonidentical receiving channels, *Izvestiya VUZ: Radioelektronika*, 42 (1), pp. 11 - 18,

Slyusar V. I. 2004. Investigation technique of the linear dynamic band of the receiving channels of a digital antenna array. *Izvestiya Vysshikh Uchebnykh Zavedenij. Radioelektronika*, 47 (9), pp. 29 - 38,

Slyusar, V., Kondratenko, Y., Shevchenko, A., Yeroshenko, T. 2024. Some Aspects of Artificial Intelligence Development Strategy for Mobile Technologies, *Journal of Mobile Multimedia*, 20_3, 525 – 554.

Striuk O., Kondratenko Y. 2021. Generative Adversarial Neural Networks and Deep Learning: Successful Cases and Advanced Approaches. *International Journal of Computing*, Vol. 20, Issue 3, , pp. 339-349.

Tijani, A. 2022. "Obstacle Avoidance Path Design for Autonomous Vehicles – A Review." *Technium J.*, 3, 64–81.

Tu, J. et al. 2022. "An Efficient Deep Learning Approach Using Improved Generative Adversarial Networks for Incomplete Information Completion of Self-driving Vehicles." *J Grid Computing*, 20, 21-28.